

An Aggregation-Suppressed Polymer Blending Strategy Enables High-Performance Organic and Quantum Dot Hybrid Solar Cells

Junwei Liu, Jiawei Qiao, Kangkang Zhou, Jingjing Wang, Ruohua Gui, Kaihu Xian, Mengyuan Gao, Hang Yin, Xiaotao Hao,* Zhihua Zhou,* and Long Ye*

Solution-processing hybrid solar cells with organics and colloidal quantum dots (CQDs) have drawn substantial attention in the past decade. Nevertheless, hybrid solar cells based on the recently developed directly synthesized CQD inks are still unexplored. Herein, a facile polymer blending strategy is put forward to enable directly synthesized CQD/polymer hybrid solar cells with a champion efficiency of 13%, taking advantage of the conjugated polymer blends with finely optimized aggregation behaviors. The spectroscopic and electrical investigations on carrier transport and recombination indicate that polymer blends can endow fast carrier transport and less recombination over the single counterparts. Moreover, the blending strategy offers a “dilution effect” for top-notch photovoltaic polymers with excessively strong aggregation tendency, resulting in moderate feature domain size and surface roughness, which afford fast hole transport and therefore high photovoltaic performance. The effectiveness of this strategy is successfully validated using two pairs of photovoltaic polymers. Accordingly, the relationships between polymer morphology, carrier transport, and photovoltaic performance are established to advance the progress of CQD/polymer hybrid solar cells. Such progress stresses that the utilization of aggregation-suppressed polymer blends is a facile approach toward the fabrication of high-efficiency organic–inorganic hybrid solar cells.

progress with a striking photovoltaic performance of $\approx 20\%$. Generally, high-performance OSC materials can seldom harvest the infrared light beyond 1000 nm, adverse to the further performance enhancement of this technology. Additionally, OSCs generally suffer from notorious degradation issues when exposed to moist air and strong solar illumination.^[6,7] Moreover, high material cost and harsh processing for the top-notch OSCs still place restrictions on their commercial applications.^[8–10]

Instead, lead chalcogenide colloidal quantum dots (CQDs) have spurred abundant research efforts due to their high stability, broad and tunable absorption spectra (≈ 1400 nm) and multiple exciton generation.^[11–18] Through the joint efforts of the community, PbS CQD solar cells can retain $\approx 80\%$ of initial efficiency after 1000 h of continuous illumination and over 90% of the initial performance after one-year of ambient storage.^[19] Moreover, PbS CQDs with broad absorption can capture the far-infrared of solar radiation, which is highly critical for the further

efficiency improvement of OSC.^[20–23] During the past decade, PbS CQD solar cells have undergone the rapid improvement of power conversion efficiency (PCE) from $\approx 3\%$ to over 13% via surface passivation and device engineering.^[24–26]

1. Introduction

Owing to high flexibility and favorable solution processing,^[1–5] organic solar cells (OSCs) have witnessed unprecedented

J. Liu, Z. Zhou
School of Environmental Science and Engineering
Tianjin University
Tianjin 300350, China
E-mail: zhuazhou@tju.edu.cn

J. Liu, K. Zhou, J. Wang, K. Xian, M. Gao, L. Ye
School of Materials Science and Engineering
Tianjin Key Laboratory of Molecular Optoelectronic Sciences
Tianjin University
Tianjin 300350, China
E-mail: yelong@tju.edu.cn

J. Qiao, R. Gui, H. Yin, X. Hao
School of Physics
Shandong University
Jinan 250100, China
E-mail: haoxt@sdu.edu.cn

J. Liu, L. Ye
State Key Laboratory of Applied Optics
Changchun Institute of Optics
Fine Mechanics and Physics
Chinese Academy of Sciences
Changchun 130033, China

 The ORCID identification number(s) for the author(s) of this article can be found under <https://doi.org/10.1002/smll.202201387>.

DOI: 10.1002/smll.202201387

With the aim to accelerate the commercialization progress of OSCs and CQD solar cells, hybrid strategy holds promising potential to be leveraged for the further improvement of OSC stability and CQD performance.^[27] Over the past five years, PbS CQD/organic hybrid solar cells with bilayer structure have made great progress with the great efficiency advance from $\approx 5\%$ to $>13\%$.^[24,28–34] Recently, Kim et al. successfully synthesized a diketopyrrolopyrrole-based polymer with high hole mobility and favorable energy level with PbS CQDs. Accordingly, the corresponding hybrid solar cells can afford the record PCE of $\approx 14\%$ and superior fill factor of 70% .^[24] Additionally, Baek et al. employed organic heterojunction (polymer donor:small molecule acceptor) to improve the stability and performance of hybrid solar cells. The resulting solar cells exhibit the PCE of 13.1% and retain over 80% of their initial PCE after 150 h of continuous operation without encapsulation.^[35]

Despite the pronounced progress, the advanced hybrid solar cells still employed the high-cost PbS CQD inks ranging from 11 to $59\text{ }\text{\$ g}^{-1}$, which hinders the commercial applications of this technology.^[36,37] To handle this challenge, Ma et al. recently developed a facile but highly effective route to synthesize one-step PbS/PbSe CQD inks with a strikingly low cost of $\approx 6\text{ }\text{\$ g}^{-1}$ and achieved desirable performance, comparable to those of CQD inks with solution-phase ligand exchange (SPLE).^[38,39] Recently, they further improved the performance of directly synthesized PbS CQD solar cells to $\approx 12.1\%$ via matrix manipulation engineering.^[40] Nevertheless, the existing directly synthesized CQD devices still employed the conventional p-type CQD hole transport layers (HTLs), which required the synthesis of CQDs with oleic acid ligand and fussy solid ligand exchange. As a result, the previous synthesis routes can't be completely eliminated. Moreover, the performance of the most advanced directly synthesized CQD solar cell (12.1%) still has a nonignorable gap

with that of SPLE inks (over 13%).^[24,41,42] Therefore, it is highly essential to employ a favorable device to fill this gap and further advance the commercial progress for the directly synthesized CQD ink. To fulfill this goal, CQD/organic hybrid strategy may contribute to the further success of this promising CQD ink. It is worth emphasizing that directly synthesized CQDs still have the obvious difference with the SPLE ones, in terms of optical and electrical properties, which require systematic investigations to clarify the detailed performance of directly synthesized CQDs/polymer heterojunction.

To further advance the commercialization progress of hybrid solar cells with directly synthesized CQD inks and deepen the understanding of CQD/polymer heterojunction, we introduced conjugated polymer materials into directly synthesized CQD devices and developed a facile polymer blending strategy for high-efficiency hybrid solar cells for the first time. A benchmark photovoltaic polymer Poly[(2,6-(4,8-bis(5-(2-ethylhexyl)-3-fluoro)thiophen-2-yl)-benzo[1,2-b:4,5-b']dithiophene))-alt-(5,5-(10,30-di-2-thienyl-50,70-bis(2-ethylhexyl)-benzo[10,20-c:40,50-c']dithiophene-4,8-dione)] (PM6) with strong temperature-dependent aggregation behaviors in solution state and well-defined fibril morphology in thin film was employed as the host polymer.^[43–46] By mixing with a weakly aggregated polymer Poly[4,8-bis(5-(2-ethylhexyl)thiophen-2-yl)benzo[1,2-b;4,5-b']dithiophene-2,6-diyl-alt-(4-(2-ethylhexyl)-3-fluorothieno[3,4-b]thiophene)-2-carboxylate-2,6-diyl)] (PTB7-Th), the derived blend with a suppressed tendency of aggregation was able to accelerate hole extraction and improve the performance of CQD/polymer hybrid solar cells (Figure 1a). We first characterized the energy level alignment, absorption and photoluminescence of the polymers and CQDs, and further performed ultrafast transient absorption to probe carrier transport between CQDs and polymers. Subsequently, the performance

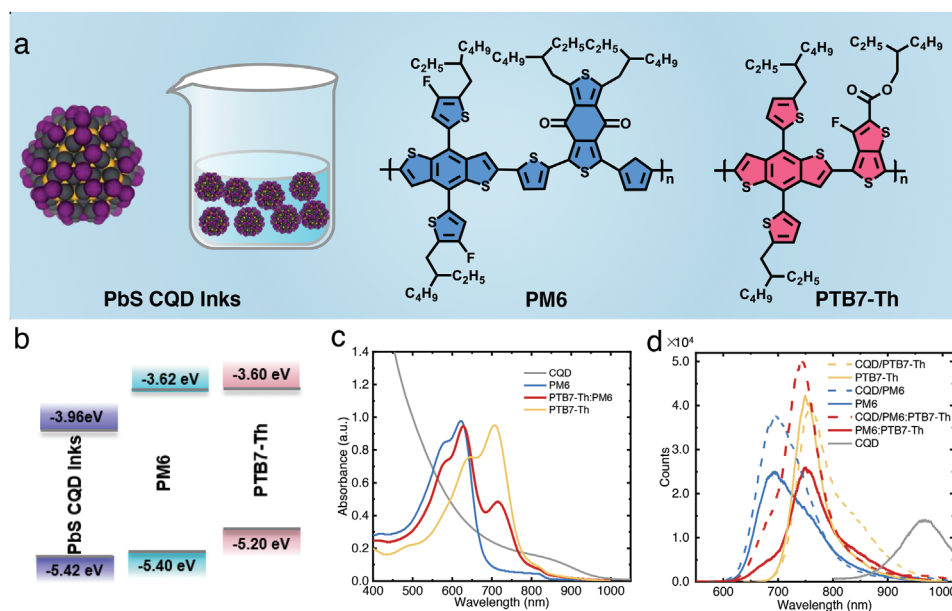


Figure 1. a) Chemical structures of PbS CQDs, and two conjugated polymers (PM6, PTB7-Th) of notable interest in the OSC community. b) Energy level diagram of PbS CQDs, PM6, and PTB7-Th. c) Absorption spectra of PbS CQDs, PM6, PTB7-Th, and the blend. d) PL spectra of PbS CQDs, PM6, PTB7-Th, the polymer blend (the PTB7-Th content of 10%), and the corresponding heterojunction including CQD/PM6, CQD/PTB7-Th, and CQD/polymer blend.

of CQD and polymer hybrid solar cells was explored to demonstrate the superiority of this polymer blending strategy and the corresponding charge transport and recombination were investigated to further explain the noteworthy performance improvement with the polymer blends. The efficiency of directly synthesized CQD/PM6:PTB7-Th thus reached 13%, which was among the best values for CQD/polymer hybrid solar cells. The polymer blending strategy was also validated in other cases of photovoltaic polymers. Moreover, the surface morphology of polymers was thoroughly characterized to further clarify the underlying mechanism of performance improvement with the developed blending strategy. With regard to the encouraging results, we further elucidated the relationship between polymer morphology, carrier transport and photovoltaic performance to guide the design of high-performance CQD and polymer hybrid solar cells.

2. Results and Discussion

2.1. CQD/Polymer Heterojunction

Due to the encouraging electrical and optical properties, directly synthesized CQDs were employed to investigate the detailed performance of CQD/polymer heterojunction. We first prepared the directly synthesized PbS CQDs with some modification according to the pioneering work by Ma group.^[39,40] The detailed synthetic route can be found in Experimental section. Except for the concise synthesis and low cost, directly synthesized CQD inks also offer long-term stability compared with the conventional CQD inks with butylamine, which endowed promising application potential. With regard to polymers, the star donor materials, PM6 and PTB7-Th were employed in this work to accelerate carrier extraction and thus improve device performance.^[4,45,47–49] Both donor materials have manifested great potential in organic solar cells and enabled the leading performance with a broad range of nonfullerene acceptors. Moreover, the two organic materials have been widely employed for hybrid solar cells, with the moderate PCE of 11.2% and 10.3%, respectively. Incorporating with the conventional CQD inks appears not to arouse the full potential of the two polymers.^[28,32] Therefore, it is highly essential to first examine the electrical and optical properties of CQD/organic heterojunction, with special attention on energy level, absorption and photoluminescence (PL).

Energy level matching is one of the prerequisites of high-performance CQD/organic hybrid solar cells. The synthesized PbS CQDs had a similar conduction band yet slightly deeper valence band, compared with the recently reported directly synthesized CQDs, which can mainly attribute to the lower synthesis temperature and deliver the slight blue shift of absorption and larger bandgap of ≈ 1.44 eV (Figure 1b,c).^[39] PM6 and PTB7-Th had the comparable conduction band of ≈ 3.6 eV; nevertheless, a markedly lower valence band was observed for PM6, which can result in significantly higher open-circuit voltage (V_{oc}). On the whole, both polymers can form a type-II heterojunction with PbS CQD, facilitating carrier extraction of CQD/organic hybrid solar cells, which can motivate the further investigation of this structure. Consistent with the

energy diagram, PTB7-Th demonstrated the noteworthy red shift of absorption with a cutoff over 800 nm, compared with that of PM6 (≈ 700 nm). In this regard, PTB7-Th can form the complementary absorption with the synthesized PbS CQD in terms of the notorious absorption valley (≈ 750 nm), which can theoretically enable higher short-circuit current density (J_{sc}). According to the above discussion, PM6 and PTB7-Th can contribute higher V_{oc} and J_{sc} , respectively. We thus wonder whether applying blends of the two polymers can combine the advantages of two single polymers and further raise the performance of CQD/organic hybrid solar cells. Motivated by this, we start to evaluate the potential of such polymer blend. The blending one indeed exhibited the broad absorption covering ≈ 400 – 800 nm, and the absorption peak ratio can be tuned facilely via altering the blending ratio.

To reveal the potential of the two polymers, we further examined the PL results of CQDs, polymers and CQD/polymer heterojunctions (Figure 1d). PbS CQDs presented a PL peak centering ≈ 1000 nm, consistent with the result from Ma group.^[40] Additionally, both PM6 and PTB7-Th offered significantly lower Stokes shifts, compared to that of PbS CQDs. Moreover, PTB7-Th delivered a narrower PL peak of ≈ 750 nm, with a marked red-shift from that of PM6. When combined with CQDs, all heterojunctions showed the single peak stemming from polymers, indicating the efficient hole transport from CQDs to polymers. More strikingly, the PL peak of CQD/PTB7-Th heterojunction presented a clear red shift from that of PTB7-Th, while that was not observed for the PM6 counterpart, demonstrating the complementary absorption. When forming a heterojunction with CQDs, the enhanced PL from the PM6 component was observed, which can infer the existence of carrier transport between PM6 and PTB7-Th, consistent with the energy landscape of the two polymers. From the above discussion, we can hold that both polymers can endow efficient carrier extraction and the polymer blends can not only realize the complementary absorption, but also form the additional energy funnel, which is expected to render faster carrier transport.

2.2. Carrier Dynamics

To check the detailed carrier transport of CQD/organic heterojunctions, we employed ultrafast transient absorption (TA) to further probe this process, focusing especially on hole migration. To this end, the samples including CQD/PM6, CQD/PTB7-Th and CQD/PM6:PTB7-Th heterojunctions were under 900 nm excitation to capture the corresponding bleach signal (Figure 2). As clearly demonstrated, all CQD/polymer heterojunctions presented the bleach signal with the broad spectral range, which was coincident with the corresponding absorption spectrums, respectively. As expected, the heterojunction with the polymer blend offered the whole bleach scope covering those of neat PTB7-Th and PM6. Additionally, the bleach signal of CQD/PTB7-Th heterojunction was clearly superior to that of PM6 counterpart in amplitude, and the blending one even afforded more encouraging intensity, which are expected to endow faster carrier transport.

More strikingly, all the heterojunctions delivered the fast build-up of bleach signal with the time scale less than 200 fs,

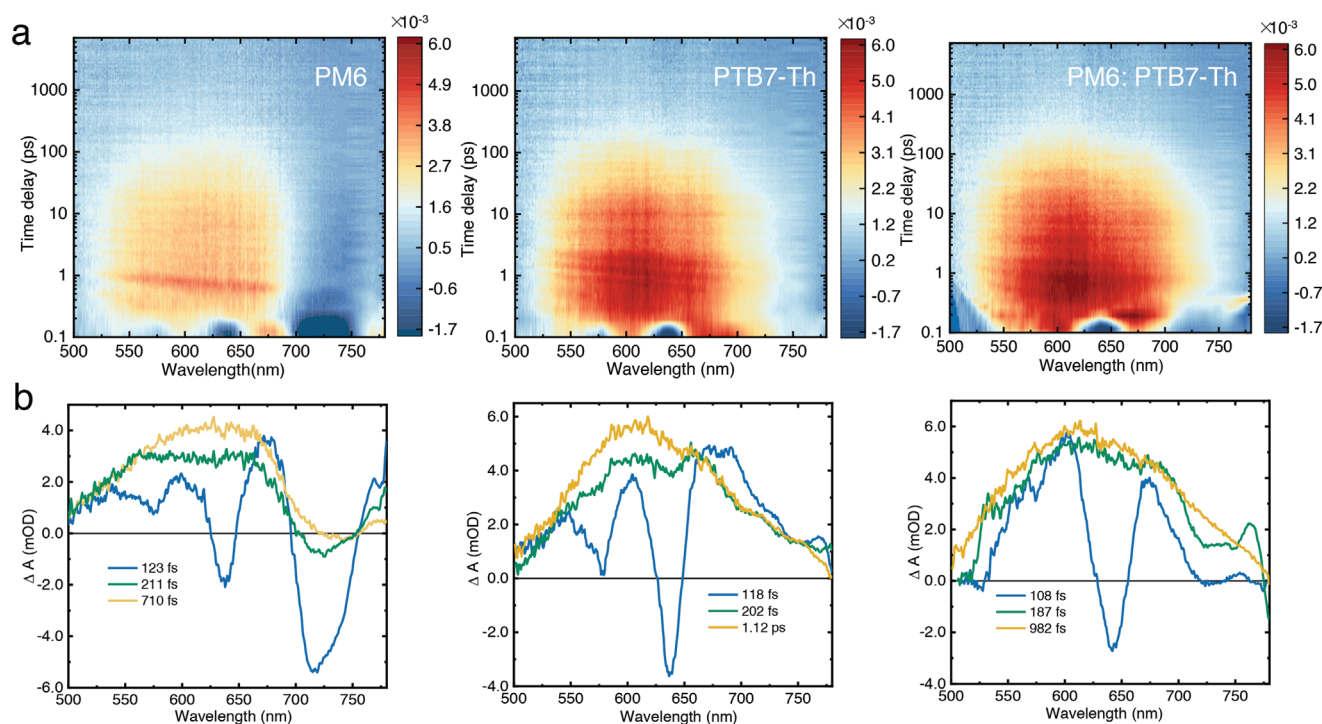


Figure 2. TA results of CQD/polymer heterojunctions. a) Spectro-temporal TA maps of CQD/ PM6, CQD/PTB7-Th, and CQD/the blending heterojunctions. b) Decay associated spectra of CQD/PM6, CQD/PTB7-Th, and CQD/the blending heterojunctions.

outperforming that of the pioneering report by Baek et al. (hundreds of picoseconds), which may stem from the thickness-dependence of bleach signal for CQD/polymer heterojunction.^[35] We can deduce the detailed hole transport process from the decay associated spectra. There first emerged two bleach signals around 610 and 670 nm in the early stage of ≈ 100 fs. Subsequently, all heterojunctions underwent fast signal enhancement and reached the maximum around 1 ps, which indicated fast hole transport from CQDs to polymers. To elaborate the carrier transport diversity of the three heterojunctions, global fitting of the TA data was implemented for the bleach signals of 610 and 670 nm and the results with double exponential fitting were plotted in Figure S1 (Supporting Information). The lifetime (τ) delivered a gradually decreasing trend with 680.2/397.3, 494.0/378.5, and 338.9/247.2 ps for three heterojunctions at 610/670 nm, respectively. The short lifetime of CQD/the blending heterojunctions (approximately half of the lifetime for PM6 one) demonstrated the more efficient hole transport with the blending strategy. Therefore, we can conclude that the polymer blending strategy can deliver significant superiority over the neat polymers in terms of hole transport, which holds great promise for high-performance hybrid CQD/polymer solar cells.

2.3. Photovoltaic Performance

Encouraged by the fast hole transport from CQDs to polymers, we proceeded to investigate the photovoltaic performance based on CQD/organic heterojunctions. We employed the commonly used structure, ITO/ZnO/PbS CQDs/Polymers/MoO_x/Ag to

build up the hybrid CQD/polymer solar cells (Figure 3a). For CQD active layer, the optimized thickness reached ≈ 400 nm, while that for polymers was ≈ 30 nm. To clarify the detailed performance of the heterojunctions with the polymer blends, we gradually raised the weight content of PTB7-Th and revealed the corresponding change trend. More specifically, PTB7-Th can enable a moderate PCE of 10.8%, with the V_{oc} , J_{sc} , and fill factor (FF) values of ≈ 0.61 V, 28.0 mA cm⁻² and 63.5%, respectively (Figure 3b). The inferior photovoltaic performance mainly stemmed from the relatively low V_{oc} , which was accordant with the slight mismatching of energy levels between CQDs and PTB7-Th. Instead, PM6 delivered a better energy level matching with CQDs, which indeed resulted in a striking V_{oc} of ≈ 0.7 V, but with slightly sacrificing J_{sc} and FF. These parameters together resulted in a PCE of $\approx 11.8\%$, higher than the previous report employing the PM6 and conventional CQD inks. The compromise on photovoltaic parameters was also consistent with the discussion on absorption and carrier dynamics based on the CQD/PM6 heterojunction.

As discussed above, the hybrid solar cells with PTB7-Th and PM6 indeed exhibited the complementary photovoltaic parameters, which further offered strong support of the blending strategy. Impressively, the blending one with 10% PTB7-Th can deliver a champion photovoltaic performance of 13% for CQD/polymer hybrid solar cells, which was to date the highest PCE for directly synthesized CQDs (Table 1). With the increase of the PTB7-Th component, the device V_{oc} gradually reduced from ≈ 0.7 V to 0.61 V, in accordance with the energy landscape of the two polymers, while the FF values presented a trend of increasing first and then decreasing, which can be attributed to the fast carrier transport of the polymer blend. Compared to

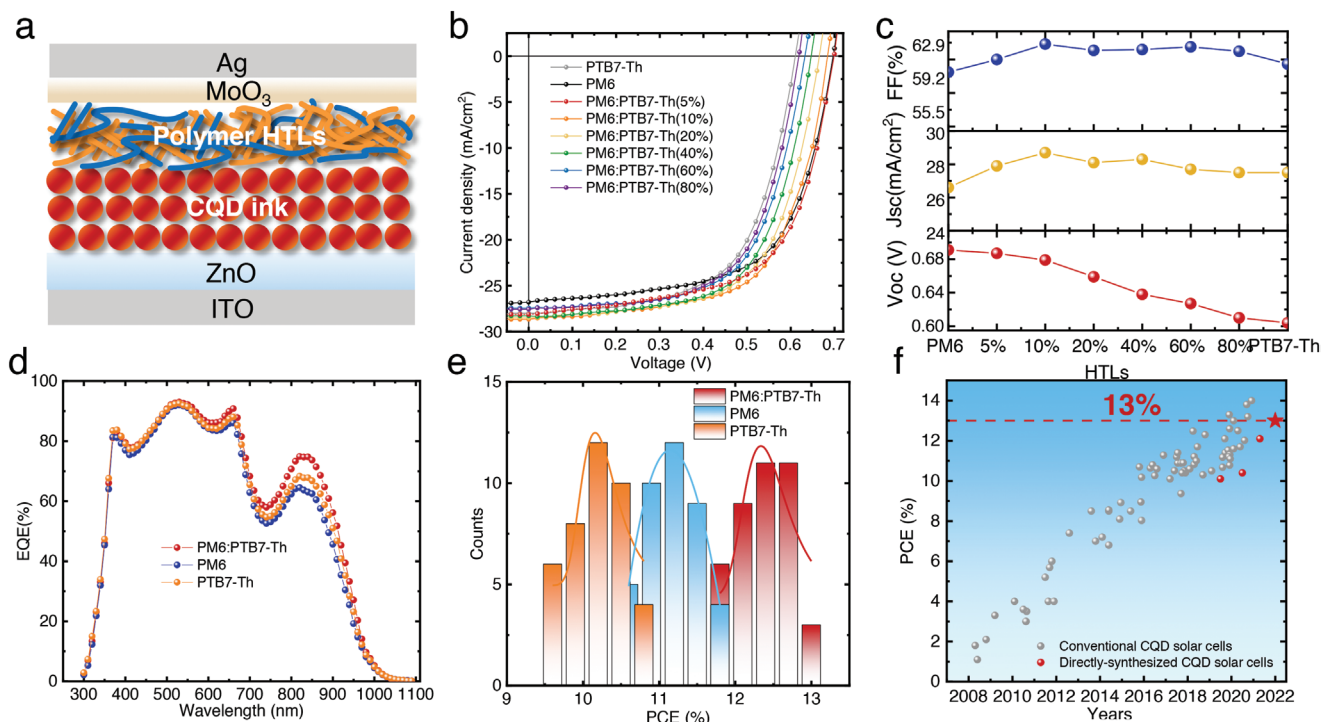


Figure 3. Photovoltaic performance CQD/polymer hybrid solar cells. a) Device structure of CQD/polymer hybrid solar cells. b) J - V curves of CQD/polymer hybrid solar cells with different polymers. c) Change trend of V_{oc} , J_{sc} and FF with the increase of the PTB7-Th component. d) EQE curves of CQD/polymer hybrid solar cells with PM6, PTB7-Th and the blending ones. e) PCE histograms of CQD/polymer hybrid solar cells. f) The progress of PBS CQD solar cells including conventional CQD inks and directly synthesized CQD inks.

the hybrid solar cells with PM6, amorphous PTB7-Th exhibited higher carrier extraction, leading to the improved FF, which may be explained from the work by Alberto Salleo et al.^[50] that short-range intermolecular aggregation was sufficient for efficient long-range charge transport. With regard to J_{sc} , the devices with the polymer blend, compared to both PM6 and PTB7-Th, presented slightly higher values, mainly due to the improvement of carrier extraction and the increase of CQD thickness (Figure 3c). Moreover, external quantum efficiency (EQE) was measured to evaluate the photoresponse of the hybrid CQD/polymer devices and the J_{sc} values calculated from EQE curves were within 5% error, compared to those derived from the corresponding J - V curves. Crucially, we can further observe the significant enhancement in terms of carrier extraction from EQE curves for PM6, PTB7-Th, and the polymer

blend (Figure 3d). On the whole, the three EQE curves all presented similar trends with regard to the bands before 600 nm, which mainly stemmed from the leading role of ZnO/CQDs heterojunction for shortwave carrier extraction. Nevertheless, for the following bands, the distinct differences of the devices with PM6, PTB7-Th, and the polymer blend were witnessed, mainly due to the increased role of hole transport. Especially for the exciton peak around 850 nm, the polymer blend can deliver an impressive EQE of $\approx 75\%$, significantly higher than $\approx 70\%$ and 65% for PTB7-Th and PM6 counterparts. The fast hole transport delivered the performance enhancement with this strategy.

To eliminate the accidental errors, 40 solar cells with PM6, PTB7-Th, and the polymer blend were prepared and the PCE distribution was plotted in Figure 3d, from which we can clearly

Table 1. Performance of the CQD/polymer hybrid solar cells with PM6, PTB7-Th, and the polymer blend.

Polymers	V_{oc} [V]	J_{sc} [mA cm^{-2}]	FF [%]	PCE [%]
PM6	0.691 ± 0.014 (0.701)	26.6 ± 0.38 (27.1)	61.5 ± 1.4 (62.0)	11.3 ± 0.4 (11.8)
PM6:PTB7-Th (5%)	0.688 ± 0.013 (0.698)	27.9 ± 0.44 (28.2)	62.9 ± 1.1 (63.7)	12.1 ± 0.3 (12.5)
PM6:PTB7-Th (10%)	0.679 ± 0.010 (0.684)	28.7 ± 0.35 (28.9)	64.6 ± 1.5 (65.8)	12.6 ± 0.3 (13.0)
PM6:PTB7-Th (20%)	0.659 ± 0.013 (0.665)	28.1 ± 0.32 (28.7)	63.9 ± 1.2 (64.9)	11.8 ± 0.4 (12.4)
PM6:PTB7-Th (40%)	0.638 ± 0.010 (0.647)	28.3 ± 0.40 (28.6)	64.5 ± 1.6 (66.0)	11.6 ± 0.5 (12.2)
PM6:PTB7-Th (60%)	0.627 ± 0.014 (0.632)	27.7 ± 0.30 (28.1)	64.3 ± 1.4 (65.4)	11.2 ± 0.3 (11.6)
PM6:PTB7-Th (80%)	0.610 ± 0.010 (0.618)	27.5 ± 0.34 (27.9)	63.8 ± 1.2 (64.6)	10.7 ± 0.4 (11.2)
PTB7-Th	0.604 ± 0.012 (0.612)	27.5 ± 0.31 (28.0)	62.4 ± 1.2 (63.5)	10.4 ± 0.3 (10.8)

observe the superiority of polymer blending strategy. With the encouraging photovoltaic results, we further outlined the progress of PbS CQD solar cells in Figure 3f and there existed rare reports with a photovoltaic performance exceeding 13%, even employing conventional CQD inks. For directly synthesized CQDs, Ma group recently developed the matrix engineering strategy, which can enable a PCE enhancement from 10.52% to 12.12%.^[40] In this work, we significantly improved the PCE record to 13% with this new strategy, which was the first result exceeding the efficiency threshold.

2.4. Charge Transport and Recombination

To gain further insight into the performance improvement with this polymer blending strategy, space charge-limited current (SCLC) hole mobility measurements were employed with a device structure of ITO/PEDOT:PSS/Polymers/MoO₃/Ag and the corresponding hole mobility was plotted in Figure 4a. Compared with the previous reports with polymer HTLs, the relatively lower mobility was mainly attributed to the removing of polymer annealing treatments, with which the hybrid CQD/polymer hybrid solar cells generally suffered from the marked performance degradation with the decrease of V_{oc} and FF (Figure S2 and Table S1, Supporting Information). Compared with the inferior performance of PM6 and PTB7-Th, the

polymer blend presented a significant improvement in hole mobility, which can reduce charge recombination, thereby explaining the corresponding increase of J_{sc} and FF. When the content of PTB7-Th reached 40%, the polymer blend delivered the champion hole mobility, eightfold that of the single PM6, which contributed to the maximum FF for all above photovoltaic devices. Despite the benefit, the higher PTB7-Th component will compromise the V_{oc} of the hybrid CQD/polymer hybrid solar cells, which can't still offer the best photovoltaic performance.

With the improved hole mobility in mind, we further investigated its impact on the charge transport of the hybrid CQD/polymer devices. The photocurrent density (J_{ph}) versus the effective voltage (V_{eff}) was performed under the illumination of AM 1.5G (Figure 4b). For all the three polymers, the J_{ph} values presented the rapid increase at the low V_{eff} below 0.4 V and subsequently reached the saturated state, indicating that the carriers in all devices achieved rapid dissociation, in accordance with the previous report on CQD/polymer solar cells.^[28,30] Nevertheless, the device with the polymer blend delivered a slightly higher saturated J_{ph} over those of PTB7-Th and PM6 counterparts, which further demonstrated the fast charge transport with polymer blending strategy. Additionally, we proceeded to reveal the charge recombination kinetics of CQD/polymer hybrid solar cells with the variation of J_{sc} and V_{oc} as a function of illumination intensity. As shown in Figure 4c, the

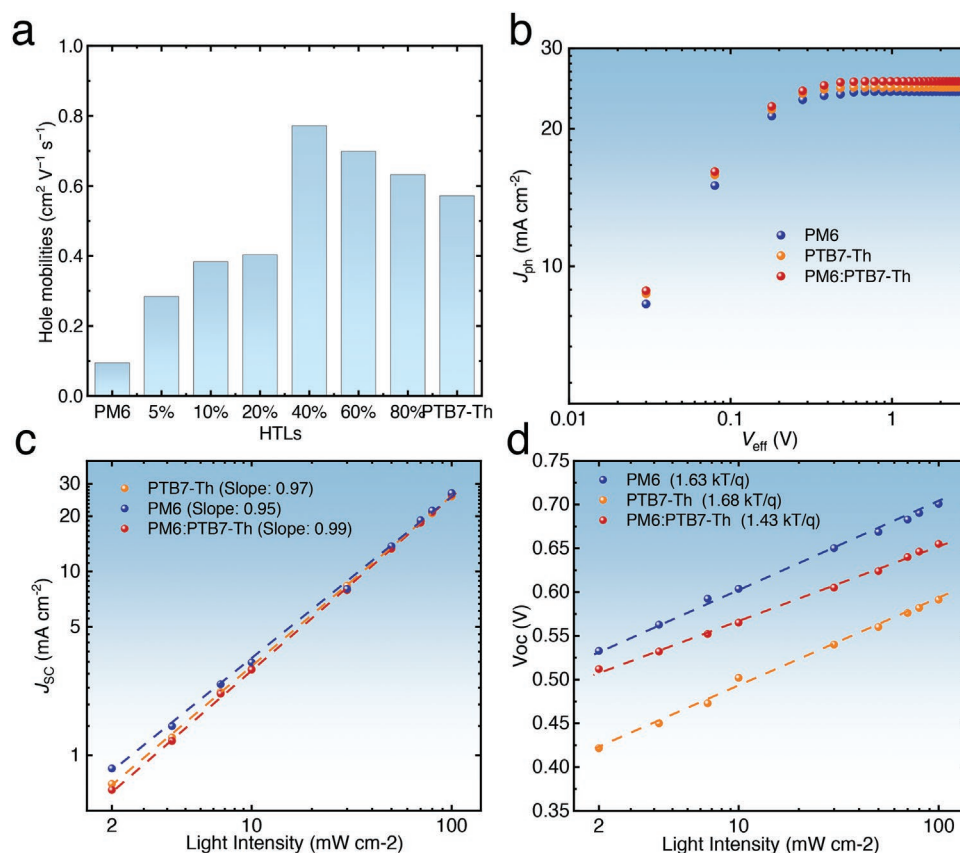


Figure 4. a) Hole mobility histograms of PM6, PTB7-Th and the polymer blend. b) Photocurrent density (J_{ph}) versus effective voltage (V_{eff}) of the devices with the above three polymers. c,d) Light-intensity dependence of J_{sc} and V_{oc} , respectively.

exponential factors of the devices with PM6, PTB7-Th, and the polymer blend are 0.95, 0.97, and 0.99, respectively, which indicated that the blending strategy can reduce bimolecular recombination, compared to the single PM6 or PTB7-Th. Additionally, light intensity dependence on V_{oc} for the three devices delivered the slope of 1.63 kT/q , 1.68 kT/q , and 1.43 kT/q for PM6, PTB7-Th, and the polymer blend, respectively, which revealed less trap-assisted carrier recombination with the polymer blending strategy. It is mainly due to the fast hole transport from CQDs to the polymer blend (Figure 4d). From the above discussion on charge transport and recombination, we took the view that the polymer blending strategy indeed endowed fast hole transport and thus reduced charge recombination, which can explain the marked enhancement of photovoltaic performance with the polymer blend.

2.5. Film Morphology

To further clarify the underlying mechanism of performance improvement with the developed blending strategy, we investigated the surface morphology of the polymers via atomic force microscopy (AFM) and transmission electron microscopy (TEM). The AFM height and phase images were plotted in Figure 5a and Figure S3 (Supporting Information), from

which we can extract the root-mean-square surface roughness (R_q) of all the polymers. PM6 and PTB7-Th presented a significant difference in surface roughness with the values of 1.2 and 0.6 nm, respectively. With the increase of the PTB7-Th component, the surface roughness of the polymer blend delivered a decreasing trend from 1.1 to 0.7 nm. We can therefore conclude that PTB7-Th are well miscible with PM6 and lead to smoother blend films, which may play a critical role in the performance enhancement of CQD/polymer hybrid solar cells. As discussed from the $J-V$ curves, the FF and PCE of the devices with the polymer blend exhibited marked improvements, compared with those of the single polymer, which indicated that moderate surface roughness may be desired morphology for high-performance CQD/polymer hybrid solar cells.

To gain more detailed insight into the optimal morphology of polymers, we employed transmission electron microscopy (TEM) to further characterize the domain size and phase separation of the above polymers. From TEM images (Figure 5a), all polymers presented short fiber aggregates and the polymer blend exhibited uniform mixing, which was in accordance with the AFM and grazing incidence wide-angle X-ray scattering (GIWAXS) results. To capture the quantitative information of domain size, a fast Fourier transform analysis was performed to generate the power spectral density (PSD) profiles of the TEM images and the results were plotted in Figure 5b. All polymers

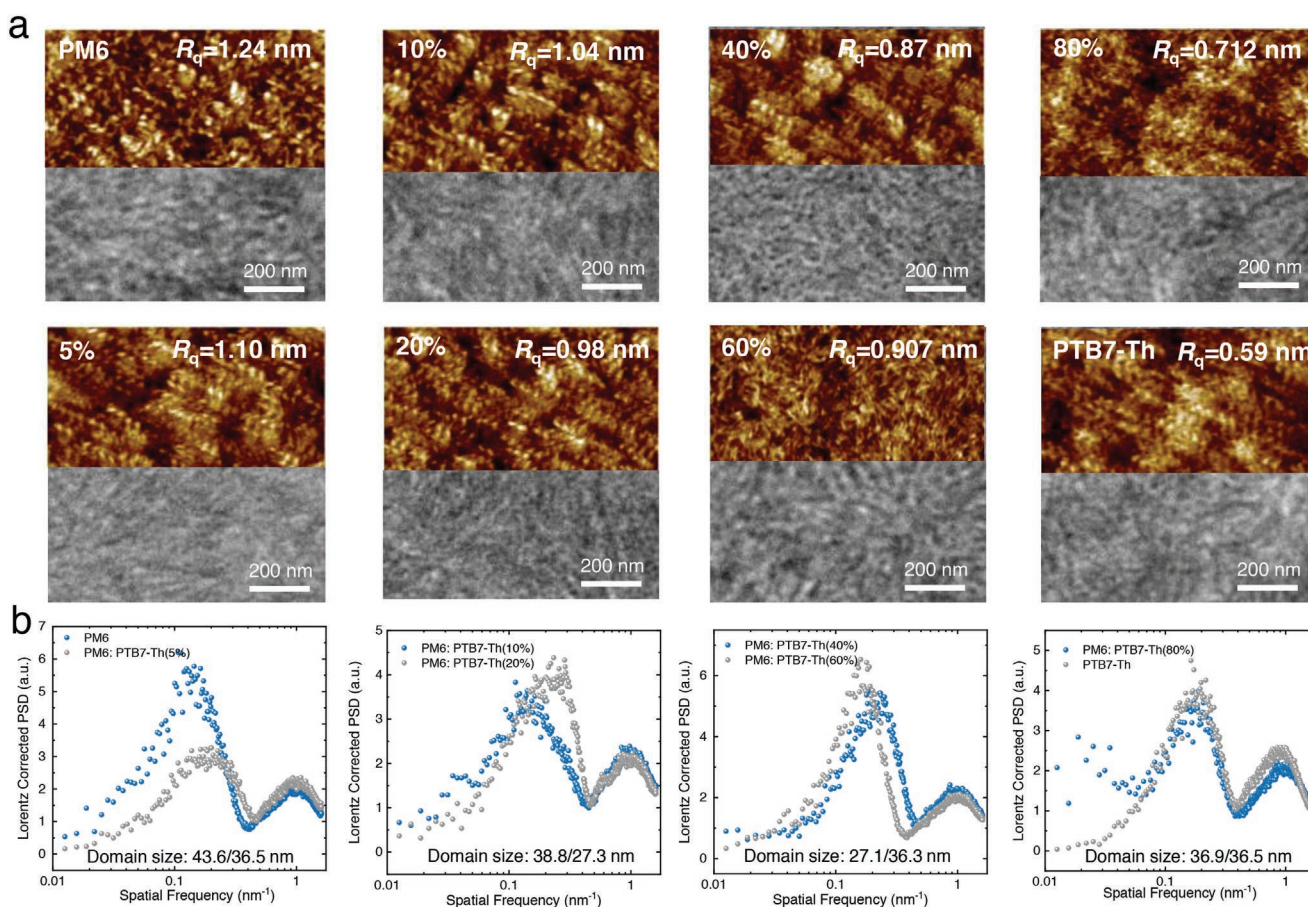


Figure 5. a) AFM and TEM images of PM6, PTB7-Th, and the polymer blends with different contents of PTB7-Th component. b) PSD profiles of the above polymers.

presented two characteristic peaks in the high- q region, one of which was around 1 nm^{-1} , corresponding to the width of the fibers in the films, $\approx 7 \text{ nm}$, while the other characteristic peak (representing the feature domain size) showed a significant difference for the polymer blend with different PTB7-Th contents. Different from the trend in AFM results, the feature domain size of the polymer blend presented a trend of first decreasing and then increasing with the component increase of PTB7-Th. When the PTB7-Th content reached 20% and 40%, the feature domain size reached the minimum of $\approx 27.0 \text{ nm}$, markedly smaller than that of 43.6 nm for the PM6 counterpart. The smaller domain size indicated the slight phase separation in the blending films, which will result in a smoother surface. Combined with the J - V results, we can infer that efficient polymer HTL required the moderate feature domain size ($\approx 30 \text{ nm}$), resulting in appropriate surface roughness and therefore fast hole transport.

2.6. Guide for High-Performance CQD/Polymer Hybrid Solar Cells

Based on the above encouraging results, we proceed to elucidate the relationship between polymer morphology, carrier transport and photovoltaic performance and further offer the guideline for high-performance CQD/polymer hybrid solar cells. From PL and TA results, we can hold that the polymer blend can enable fast carrier transport for CQD/polymer heterojunctions, which can also gain evidence from the investigation of the devices with the three polymers in terms of charge transport and recombination. As confirmed, the polymer blend indeed enabled efficient charge transport and thus reduced charge recombination for hybrid CQD/polymer devices, which can significantly enhance photovoltaic performance. The underlying mechanism for the improvement of these parameters may stem from morphology optimization via the blending strategy. From AFM and TEM images, we can infer that polymer PM6 had relatively higher crystallization compared to that of PTB7-Th (nearly amorphous), therefore leading to larger feature domain size and rougher film surface, which resulted in slower carrier transport and moderate photovoltaic performance. The clear temperature-dependent aggregation behaviors of PM6 in dilute solution offered the clear evidence of its high aggregation tendency, which may explain the moderate carrier extraction (Figure 6a,b).^[49,51] When introducing the guest polymer with significantly lower degrees of aggregation into the host polymer, a magical “dilution effect” was yielded with the reduced feature domain size and surface roughness, therefore more favorable morphology can be created for high-performance CQD/polymer hybrid solar cells (Figure 6c).

Based on the “dilution effect,” our polymer blending strategy may exhibit broad application potential in high-performance CQD/organic hybrid solar cells. Another promising photovoltaic polymer with low aggregation tendency, Poly{(4,8-bis(5-(2-ethylhexyl)thiophen-2-yl)benzo[1,2-b:4,5-b']dithiophene-co-4,8-di(thien-2-yl)-2-(6-(1,1,1,3,5,5,5-heptamethyltrisiloxan-3-yl)hexyl)-6-octyl[1,2,3]triazolo[4,5-f]isoindole-5,7(2H,6H)-dione)} (PTzBi-Si)^[52] were sought out for hybrid solar cells and the absorption and energy landscape were plotted in Figure S4

(Supporting Information). It can be clearly seen that PTzBi-Si can deliver a PCE of $\approx 8.8\%$, respectively, while the value surpasses 12% when blending with PM6, which also presented the superiority of the developed strategy (Figure S5 and Table S2, Supporting Information). We proceeded to investigate the surface morphology of the polymer system, PM6:PTzBi-Si. AFM images were plotted in Figure S6 (Supporting Information), from which we can confirm that the polymer blend indeed delivered moderate surface roughness and optimized domain sizes, which can enable markedly higher photovoltaic performance. Additionally, small-molecule acceptors may also exhibit the “dilution effect”, when introduced into highly crystalline polymers, e.g., Poly(3-hexylthiophene-2,5-diyl) (P3HT)^[53] and Poly[[6,7-difluoro[(2-hexyldecyl)oxy]-5,8-quinoxalinediyl]-2,5-thiophenediyl] (PTQ10).^[54] We can also employ the quantitative analysis method to further reveal the mixing behaviors and the corresponding morphology for the blends.^[55,56]

3. Conclusions

With the aim to endow the simultaneous realization of performance improvement and easy processing, this work introduced conjugated polymers, PM6 and PTB7-Th into directly synthesized CQD devices and put forward a promising polymer blending strategy to further enhance the performance of CQD/polymer hybrid solar cells. The polymers and directly synthesized CQDs presented favorable energy level alignments and PTB7-Th can form the complementary absorption with the synthesized PbS CQDs. PL and TA results indicated that the polymer blending strategy enabled fast hole transport from CQDs to polymers, which were expected to deliver the markedly increased photovoltaic performance. Indeed, the devices with the polymer blend can achieve a champion PCE of over 13%, significantly higher than those of the single counterparts. Moreover, the investigation on charge transport and recombination further demonstrated the superiority of the polymer blend with fast hole transport and therefore less charge recombination.

Additionally, the surface morphology of the polymer components and polymer blends was investigated to further clarify the underlying mechanism of performance improvement with the blending strategy. The results revealed that the PTB7-Th component can reduce the feature domain size and surface roughness of PM6, therefore resulting in favorable morphology for high-performance CQD/polymer hybrid solar cells. We further established the relationship between polymer morphology, carrier transport and photovoltaic performance to guide the design of high-performance CQD/polymer hybrid solar cells. The morphological and performance superiority benefitted from this blending strategy were also validated with some other photovoltaic polymers. Consequently, our work not only breaks through the efficiency of directly synthesized CQD solar cells to 13%, but also simultaneously enriches the guideline for constructing cost-effective, efficient, and reproducible CQD/polymer hybrid solar cells. Moving forward, blending the photovoltaic polymers with the recently developed high mobility polymer semiconductors^[57–59] and novel polymer acceptors^[60–64] might offer new opportunities for the optimization of directly synthesized CQD solar cells and photodetectors.^[65,66]

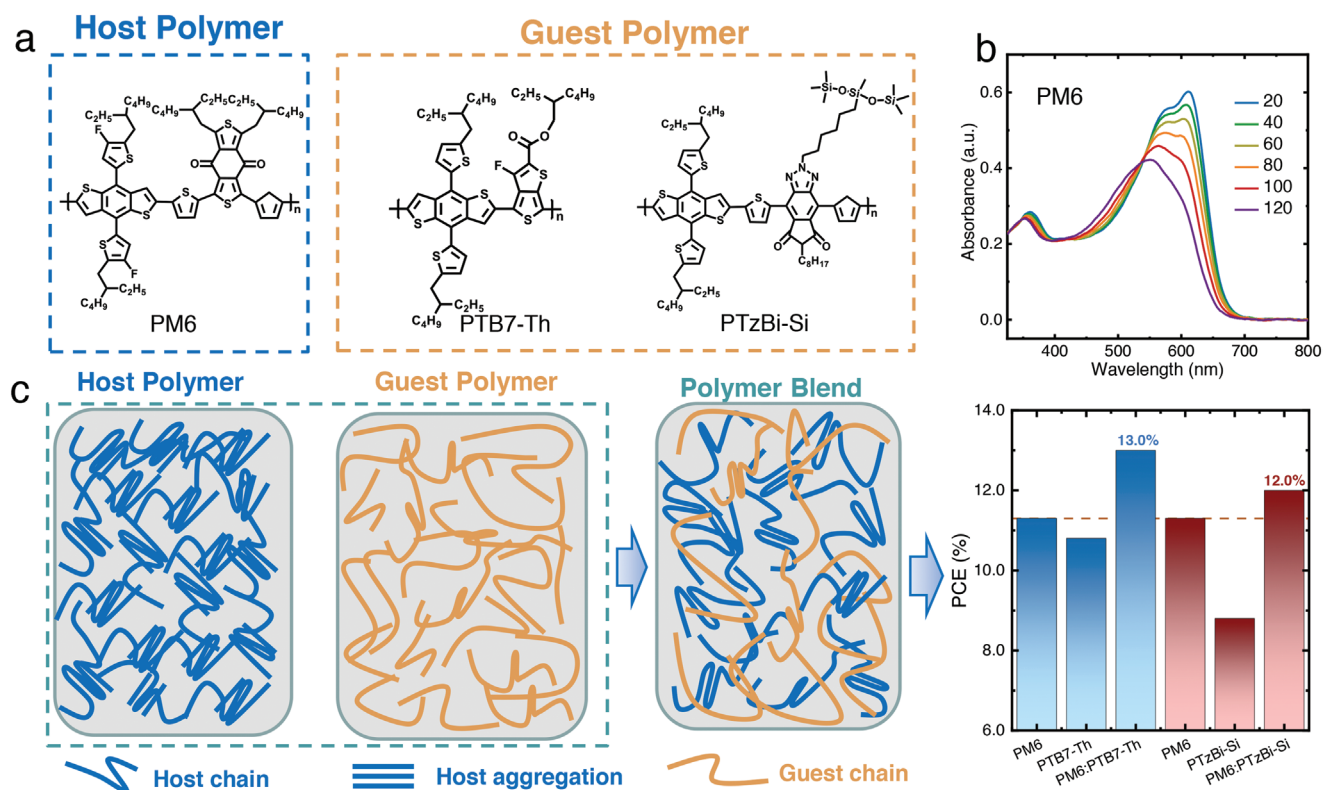


Figure 6. a) Chemical structures of the host polymer PM6 and three guest polymers. b) Absorption spectra of PM6 in dilute solution with the increase of temperature. c) Schematic illustrations of the morphological superiority of the model polymer blend over the individual polymers in CQD/polymer hybrid solar cells. The plots of PCEs for the blend systems and their constituted polymers are provided for comparisons.

4. Experimental Section

PbS CQD Synthesis: PbS CQDs were synthesized based on a previous report with some modifications.^[40] 6 mmol PbI₂ and 1 mmol diphenyl thiourea (DPhTA) were dissolved in 9 mL dimethylformamide (DMF) with stirring under argon at a control temperature of ≈20 °C. After all solid reagents were dissolved within ≈20 min, 1 mL butylamine (BA) was quickly injected to trigger the CQD synthesis reaction. After reacting ≈9 min, 0.7 mmol tetrabutylammonium iodide (TBAI) in 1 mL DMF was injected into the reaction system and subsequently, the solution was centrifuged for 5 min at 12 000 rpm with the addition of 25 mL toluene. After vacuum drying, the prepared CQDs were stored in glove box for use.

Photovoltaic Device Fabrication: The photovoltaic devices employed the commonly used structure, ITO/ZnO/PbS CQDs/Polymers/MoO_x/Ag. Sol-gel ZnO was synthesized according to the previous report and magnesium acetate tetrahydrate was used to slightly dope sol-gel ZnO, which have been demonstrated to facilitate the performance improvement of CQD solar cells.^[67,68] The MgZnO sol-gel was spin-coated on ITO glass substrates at 3000 rpm for 40 s, and this process was repeated three times resulting in a total thickness of 150 nm. Subsequently, the prepared CQDs in DMF (1000 mg mL⁻¹) was spin-coated with different speeds to form 300–350 nm CQD films in glove box, followed by 75 °C annealing for 15 min. For polymers, PM6, PTB7-Th, and the polymer blends in chlorobenzene (6 mg mL⁻¹) were spin-coated at 2000 rpm. Note that 0.05% 1,8-dioctane (DIO) was added into the polymer blends. After that, MoO_x/Ag (8 nm/120 nm) as anode was thermally evaporated under low pressure (<10⁻⁴ Pa).

Characterizations: The UV-vis-NIR absorption spectrum were measured by a Shimadzu UV-3600 Plus spectrometer. Photoluminescence (PL) was recorded by the FLIM equipment consisting of the confocal optical microscope (Nanofinder FLEX2, Tokyo Instruments, Inc.). Femtosecond transient absorption spectroscopy

measurements were performed on an Ultrafast Helios pump-probe system in collaboration with a regenerative amplified laser system from Coherent. The energy of pump pulse was measured and calibrated by a power meter (PM400, Thorlabs). *J*-*V* curves of the devices with different polymers were measured by Keithley 2400 source meter under the standard AM 1.5G spectrum from an AAA solar simulator (SS-F5-3A, Enli Technology Co. Ltd, Taiwan). The light intensity was calibrated with a standard photovoltaic cell equipped with a KG5 filter. EQE curves were measured by QE-R, Enli Technology Co. Ltd. Surface morphology of the polymers were measured by atomic force microscope (AFM, Bruker Multimode 8). The corresponding TEM images were collected JEOL JEM-2100PLUS electron microscope. GIWAXS characterizations are consistent with our prior publication².

Supporting Information

Supporting Information is available from the Wiley Online Library or from the author.

Acknowledgements

The authors would like to especially acknowledge the financial support by the Open Fund of State Key Laboratory of Applied Optics (No. SKLAO2021001A17) and the Peiyang Scholar Program of Tianjin University. L.Y. also gratefully acknowledges the National Natural Science Foundation of China (No. 52073207) for support. J.L. would like to acknowledge Shanghai Tongji Gao Tingyao Environmental Protection Technology Development Foundation for support. GIWAXS data were acquired at Shanghai Synchrotron Radiation Facility (SSRF), beamline BL14B1, beamline BL16B1 and Beijing Synchrotron Radiation Facility

(BSRF), beamline 1W1A. Prof. Yanhou Geng is appreciated for providing the fume hood for quantum dot synthesis.

Conflict of Interest

The authors declare no conflict of interest.

Author Contributions

L.Y. and J.L. conceived the idea and designed the experimental details. J.L. performed the device fabrication and characterization with the assistance of J.W. K.Z., K.X., and M.G. conducted morphology characterizations. J.Q. performed the TA characterizations under the direction of X.H. R.G. and H.Y. performed the PL measurements. J.L. analyzed the data and wrote the manuscript with the input from L.Y., H.Y., Z.Z., and X.H. Z.Z. and L.Y. directed the research. All authors contributed to the editing of this manuscript.

Data Availability Statement

The data that support the findings of this study are available from the corresponding author upon reasonable request.

Keywords

aggregation, colloidal quantum dots, hybrid solar cells, photovoltaic polymers, polymer blends

Received: March 3, 2022

Revised: March 27, 2022

Published online: April 13, 2022

- [1] L. Zhan, S. Li, Y. Li, R. Sun, J. Min, Z. Bi, W. Ma, Z. Chen, G. Zhou, H. Zhu, M. Shi, L. Zuo, H. Chen, *Joule* **2022**, *6*, 662.
- [2] Z. Peng, K. Xian, Y. Cui, Q. Qi, J. Liu, Y. Xu, Y. Chai, C. Yang, J. Hou, Y. Geng, L. Ye, *Adv. Mater.* **2021**, *33*, 2106732.
- [3] Z. Peng, K. Jiang, Y. Qin, M. Li, N. Balar, B. T. O'Connor, H. Ade, L. Ye, Y. Geng, *Adv. Energy Mater.* **2021**, *11*, 2003506.
- [4] J. Yuan, Y. Zhang, L. Zhou, G. Zhang, H. L. Yip, T. K. Lau, X. Lu, C. Zhu, H. Peng, P. A. Johnson, M. Leclerc, Y. Cao, J. Ulanski, Y. Li, Y. Zou, *Joule* **2019**, *3*, 1140.
- [5] L. Ye, H. Ke, Y. Liu, *Trends Chem.* **2021**, *3*, 1074.
- [6] Q. Burlingame, X. Huang, X. Liu, C. Jeong, C. Coburn, S. R. Forrest, *Nature* **2019**, *573*, 394.
- [7] Q. Burlingame, M. Ball, Y. L. Loo, *Nat. Energy* **2020**, *5*, 947.
- [8] Q. Wang, Y. Qin, M. Li, L. Ye, Y. Geng, *Adv. Energy Mater.* **2020**, *10*, 2002572.
- [9] J. Ren, P. Bi, J. Zhang, J. Liu, J. Wang, Y. Xu, Z. Wei, S. Zhang, J. Hou, *Natl. Sci. Rev.* **2021**, *8*, nwab031.
- [10] C. Yang, S. Zhang, J. Ren, M. Gao, P. Bi, L. Ye, J. Hou, S. Zhang, L. Ye, J. Hou, *Energy Environ. Sci.* **2020**, *13*, 2864.
- [11] M. Liu, Y. Chen, C. S. Tan, R. Quintero-Bermudez, A. H. Proppe, R. Munir, H. Tan, O. Voznyy, B. Scheffel, G. Walters, A. P. T. Kam, B. Sun, M. J. Choi, S. Hoogland, A. Amassian, S. O. Kelley, F. P. García de Arquer, E. H. Sargent, *Nature* **2019**, *570*, 96.
- [12] Y. Cao, A. Stavrinadis, T. Lasanta, D. So, G. Konstantatos, *Nat. Energy* **2016**, *1*, 16035.
- [13] M. Yuan, M. Liu, E. H. Sargent, *Nat. Energy* **2016**, *1*, 16016.
- [14] X. Lan, S. Masala, E. H. Sargent, *Nat. Mater.* **2014**, *13*, 233.
- [15] C. H. M. Chuang, P. R. Brown, V. Bulović, M. G. Bawendi, *Nat. Mater.* **2014**, *13*, 796.
- [16] J. Xu, O. Voznyy, M. Liu, A. R. Kirmani, G. Walters, R. Munir, M. Abdelsamie, A. H. Proppe, A. Sarkar, F. P. García De Arquer, M. Wei, B. Sun, M. Liu, O. Ouellette, R. Quintero-Bermudez, J. Li, J. Fan, L. Quan, P. Todorovic, H. Tan, S. Hoogland, S. O. Kelley, M. Stefik, A. Amassian, E. H. Sargent, *Nat. Nanotechnol.* **2018**, *13*, 456.
- [17] J. H. Healy, J. D. Bredehoeft, R. L. Wesson, H. Helm, H. Poitrenaud, A. Etchecopar, R. L. Wesson, W. W. Rubey, N. Lapusta, J. Rice, P. Bernard, A. Kohli, I. Das, M. McClure, *Science* **2015**, *348*, 1226.
- [18] O. E. Semonin, A. J. Nozik, M. C. Beard, *Science* **2011**, *334*, 1530.
- [19] S. W. Baek, S. H. Lee, J. H. Song, C. Kim, Y. S. Ha, H. Shin, H. Kim, S. Jeong, J. Y. Lee, *Energy Environ. Sci.* **2018**, *11*, 2078.
- [20] Y. Kim, F. Che, J. W. Jo, J. Choi, F. P. García de Arquer, O. Voznyy, B. Sun, J. Kim, M. J. Choi, R. Quintero-Bermudez, F. Fan, C. S. Tan, E. Bladt, G. Walters, A. H. Proppe, C. Zou, H. Yuan, S. Bals, J. Hofkens, M. B. J. Roeloffs, S. Hoogland, E. H. Sargent, *Adv. Mater.* **2019**, *31*, 1805580.
- [21] J. Z. Fan, N. T. Andersen, M. Biondi, P. Todorović, B. Sun, O. Ouellette, J. Abed, L. K. Sagar, M. J. Choi, S. Hoogland, F. P. G. de Arquer, E. H. Sargent, *Adv. Mater.* **2019**, *31*, 1904304.
- [22] B. Sun, O. Ouellette, F. P. García de Arquer, O. Voznyy, Y. Kim, M. Wei, A. H. Proppe, M. I. Saidaminov, J. Xu, M. Liu, P. Li, J. Z. Fan, J. W. Jo, H. Tan, F. Tan, S. Hoogland, Z. H. Lu, S. O. Kelley, E. H. Sargent, *Nat. Commun.* **2018**, *9*, 4003.
- [23] M. M. Tavakoli, H. T. Dastjerdi, P. Yadav, D. Prochowicz, H. Si, R. Tavakoli, *Adv. Funct. Mater.* **2021**, *31*, 2010623.
- [24] H. Il Kim, S. W. Baek, H. J. Cheon, S. U. Ryu, S. Lee, M. J. Choi, K. Choi, M. Biondi, S. Hoogland, F. P. G. de Arquer, S. K. Kwon, Y. H. Kim, T. Park, E. H. Sargent, *Adv. Mater.* **2020**, *32*, 2004985.
- [25] B. Kim, S. W. Baek, C. Kim, J. Kim, J. Y. Lee, *Adv. Energy Mater.* **2022**, *12*, 2102689.
- [26] B. Sun, A. Johnston, C. Xu, M. Wei, Z. Huang, Z. Jiang, H. Zhou, Y. Gao, Y. Dong, O. Ouellette, X. Zheng, J. Liu, M. J. Choi, Y. Gao, S. W. Baek, F. Laquai, O. M. Bakr, D. Ban, O. Voznyy, F. P. García de Arquer, E. H. Sargent, *Joule* **2020**, *4*, 1542.
- [27] J. Liu, K. Xian, L. Ye, Z. Zhou, *Adv. Mater.* **2021**, *33*, 2008115.
- [28] Y. Xue, F. Yang, J. Yuan, Y. Zhang, M. Gu, Y. Xu, X. Ling, Y. Wang, F. Li, T. Zhai, J. Li, C. Cui, Y. Chen, W. Ma, *ACS Energy Lett.* **2019**, *4*, 2850.
- [29] M. Al Mubarak, F. T. A. Wibowo, H. Aqoma, N. Vamsi Krishna, W. Lee, D. Y. Ryu, S. Cho, I. H. Jung, S. Y. Jang, *ACS Energy Lett.* **2020**, *5*, 3452.
- [30] Y. Zhang, Y. Kan, K. Gao, M. Gu, Y. Shi, X. Zhang, Y. Xue, X. Zhang, Z. Liu, Y. Zhang, J. Yuan, W. Ma, A. K. Y. Jen, *ACS Energy Lett.* **2020**, *5*, 2335.
- [31] D. C. J. Neo, N. Zhang, Y. Tazawa, H. Jiang, G. M. Hughes, C. R. M. Grovenor, H. E. Assender, A. A. R. Watt, *ACS Appl. Mater. Interfaces* **2016**, *8*, 12101.
- [32] M. Al Mubarak, H. Aqoma, F. T. A. Wibowo, W. Lee, H. M. Kim, D. Y. Ryu, J. W. Jeon, S. Y. Jang, *Adv. Energy Mater.* **2020**, *10*, 1902933.
- [33] H. Il Kim, J. Lee, M. J. Choi, S. U. Ryu, K. Choi, S. Lee, S. Hoogland, F. P. G. de Arquer, E. H. Sargent, T. Park, *Adv. Energy Mater.* **2020**, *10*, 2002084.
- [34] H. Aqoma, M. Al Mubarak, W. Lee, W. T. Hadmojo, C. Park, T. K. Ahn, D. Y. Ryu, S. Y. Jang, *Adv. Energy Mater.* **2018**, *8*, 1800572.
- [35] S. W. Baek, S. Jun, B. Kim, A. H. Proppe, O. Ouellette, O. Voznyy, C. Kim, J. Kim, G. Walters, J. H. Song, S. Jeong, H. R. Byun, M. S. Jeong, S. Hoogland, F. P. García de Arquer, S. O. Kelley, J. Y. Lee, E. H. Sargent, *Nat. Energy* **2019**, *4*, 969.
- [36] J. Jean, J. Xiao, R. Nick, N. Moody, M. Nasilowski, M. Bawendi, V. Bulović, *Energy Environ. Sci.* **2018**, *11*, 2295.

- [37] H. Lee, H. J. Song, M. Shim, C. Lee, *Energy Environ. Sci.* **2020**, *13*, 404.
- [38] Y. Liu, F. Li, G. Shi, Z. Liu, X. Lin, Y. Shi, Y. Chen, X. Meng, Y. Lv, W. Deng, X. Pan, W. Ma, *ACS Energy Lett.* **2020**, *5*, 3797.
- [39] Y. Wang, Z. Liu, N. Huo, F. Li, M. Gu, X. Ling, Y. Zhang, K. Lu, L. Han, H. Fang, A. G. Shulga, Y. Xue, S. Zhou, F. Yang, X. Tang, J. Zheng, M. Antonietta Loi, G. Konstantatos, W. Ma, *Nat. Commun.* **2019**, *10*, 5136.
- [40] F. Li, Y. Liu, G. Shi, W. Chen, R. Guo, D. Liu, Y. Zhang, Y. Wang, X. Meng, X. Zhang, Y. Lv, W. Deng, Q. Zhang, Y. Shi, Y. Chen, K. Wang, Q. Shen, Z. Liu, P. Müller-buschbaum, W. Ma, *Adv. Funct. Mater.* **2021**, *31*, 2104457.
- [41] M. Biondi, M. J. Choi, O. Ouellette, S. W. Baek, P. Todorović, B. Sun, S. Lee, M. Wei, P. Li, A. R. Kirmani, L. K. Sagar, L. J. Richter, S. Hoogland, Z. H. Lu, F. P. García de Arquer, E. H. Sargent, *Adv. Mater.* **2020**, *32*, 1906199.
- [42] M. J. Choi, F. P. García de Arquer, A. H. Proppe, A. Seifitokaldani, J. Choi, J. Kim, S. W. Baek, M. Liu, B. Sun, M. Biondi, B. Scheffel, G. Walters, D. H. Nam, J. W. Jo, O. Ouellette, O. Voznyy, S. Hoogland, S. O. Kelley, Y. S. Jung, E. H. Sargent, *Nat. Commun.* **2020**, *11*, 103.
- [43] M. Zhang, L. Zhu, G. Zhou, T. Hao, C. Qiu, Z. Zhao, Q. Hu, B. W. Larson, H. Zhu, Z. Ma, Z. Tang, W. Feng, Y. Zhang, T. P. Russell, F. Liu, *Nat. Commun.* **2021**, *12*, 309.
- [44] T. Shan, Y. Zhang, Y. Wang, Z. Xie, Q. Wei, J. Xu, M. Zhang, C. Wang, Q. Bao, X. Wang, C. C. Chen, J. Huang, Q. Chen, F. Liu, L. Chen, H. Zhong, *Nat. Commun.* **2020**, *11*, 5585.
- [45] C. Li, J. Zhou, J. Song, J. Xu, H. Zhang, X. Zhang, J. Guo, L. Zhu, D. Wei, G. Han, J. Min, Y. Zhang, Z. Xie, Y. Yi, H. Yan, F. Gao, F. Liu, Y. Sun, *Nat. Energy* **2021**, *6*, 605.
- [46] Z. Zheng, H. Yao, L. Ye, Y. Xu, S. Zhang, J. Hou, *Mater. Today* **2020**, *35*, 115.
- [47] Y. Cui, Y. Wang, J. Bergqvist, H. Yao, Y. Xu, B. Gao, C. Yang, S. Zhang, O. Inganäs, F. Gao, J. Hou, *Nat. Energy* **2019**, *4*, 768.
- [48] L. Ye, Y. Xiong, M. Zhang, X. Guo, H. Guan, Y. Zou, H. Ade, *Nano Energy* **2020**, *77*, 105310.
- [49] L. Ye, S. Li, X. Liu, S. Zhang, M. Ghasemi, Y. Xiong, J. Hou, H. Ade, *Joule* **2019**, *3*, 443.
- [50] R. Noriega, J. Rivnay, K. Vandewal, F. P. V. Koch, N. Stingelin, P. Smith, M. F. Toney, A. Salleo, *Nat. Mater.* **2013**, *12*, 1038.
- [51] Z. Peng, L. Ye, H. Ade, *Mater. Horiz.* **2022**, *9*, 577.
- [52] B. Fan, L. Ying, P. Zhu, F. Pan, F. Liu, J. Chen, F. Huang, Y. Cao, *Adv. Mater.* **2017**, *29*, 1703906.
- [53] Y. Zhong, A. R. Kirmani, X. Lan, J. Carpenter, A. Chew, O. Awartani, L. Yu, M. R. Niazi, O. Voznyy, H. Hu, G. Ngongang Ndjawa, M. L. Tietze, A. Salleo, H. Ade, E. H. Sargent, A. Amassian, *J. Mater. Chem. A* **2022**, *10*, 1788.
- [54] C. Sun, F. Pan, H. Bin, J. Zhang, L. Xue, B. Qiu, Z. Wei, Z. G. Zhang, Y. Li, *Nat. Commun.* **2018**, *9*, 743.
- [55] M. Gao, W. Wang, J. Hou, L. Ye, *Aggregate* **2021**, *2*, <https://doi.org/10.1002/agt2.46>.
- [56] L. Ye, H. Hu, M. Ghasemi, T. Wang, B. A. Collins, J. H. Kim, K. Jiang, J. H. Carpenter, H. Li, Z. Li, T. McAfee, J. Zhao, X. Chen, J. L. Y. Lai, T. Ma, J. L. Bredas, H. Yan, H. Ade, *Nat. Mater.* **2018**, *17*, 253.
- [57] Z. Wang, M. Gao, C. He, W. Shi, Y. Deng, Y. Han, L. Ye, Y. Geng, *Adv. Mater.* **2022**, *34*, 2108255.
- [58] Z. Ni, H. Wang, H. Dong, Y. Dang, Q. Zhao, X. Zhang, *Nat. Chem.* **2019**, *11*, 271.
- [59] X. Guo, A. Facchetti, *Nat. Mater.* **2020**, *19*, 922.
- [60] H. Sun, H. Yu, Y. Shi, J. Yu, Z. Peng, X. Zhang, B. Liu, J. Wang, R. Singh, J. Lee, Y. Li, Z. Wei, Q. Liao, Z. Kan, L. Ye, H. Yan, F. Gao, X. Guo, *Adv. Mater.* **2020**, *32*, 2004183.
- [61] Z. Luo, T. Liu, R. Ma, Y. Xiao, L. Zhan, G. Zhang, H. Sun, F. Ni, G. Chai, J. Wang, C. Zhong, Y. Zou, X. Guo, X. Lu, H. Chen, H. Yan, C. Yang, *Adv. Mater.* **2020**, *32*, 2005942.
- [62] K. Zhou, K. Xian, L. Ye, *InfoMat* **2022**, <https://doi.org/10.1002/inf2.12270>.
- [63] Z. Zhang, Y. Yang, J. Yao, L. Xue, S. Chen, X. Li, W. Morrison, C. Yang, Y. Li, *Angew. Chem. Int. Ed.* **2017**, *56*, 13503.
- [64] J. Du, K. Hu, L. Meng, I. Angunawela, J. Zhang, S. Qin, A. Liebman-Pelaez, C. Zhu, Z. Zhang, H. Ade, Y. Li, *Angew. Chem., Int. Ed.* **2020**, *59*, 15181.
- [65] C. Wang, X. Zhang, W. Hu, *Chem. Soc. Rev.* **2020**, *49*, 653.
- [66] J. Liu, M. Gao, J. Kim, Z. Zhou, D. S. Chung, H. Yin, L. Ye, *Mater. Today* **2021**, *51*, 475.
- [67] Z. L. Teh, L. Hu, Z. Zhang, A. R. Gentle, Z. Chen, Y. Gao, L. Yuan, Y. Hu, T. Wu, R. J. Patterson, S. Huang, *ACS Appl. Mater. Interfaces* **2020**, *12*, 22751.
- [68] X. Zhang, P. K. Santra, L. Tian, M. B. Johansson, H. Rensmo, E. M. J. Johansson, *ACS Nano* **2017**, *11*, 8478.